AFRL-RX-WP-JA-2015-0104

A CRYSTAL-PLASTICITY FEM STUDY ON EFFECTS OF SIMPLIFIED GRAIN REPRESENTATION AND MESH TYPES ON MESOSCOPIC PLASTICITY HETEROGENEITIES (POSTPRINT)

M.A. Groeber, T.J. Turner, D.M. Dimiduk, C.F. Woodward, and M.D. Uchic
AFRL/RXCM

Y.S. Choi and T.A. Parthasarathy
UES, Inc.

APRIL 2014
Interim Report

AIR FORCE RESEARCH LABORATORY
MATERIALS AND MANUFACTURING DIRECTORATE
WRIGHT-PATTERSON AIR FORCE BASE OH 45433-7750
AIR FORCE MATERIEL COMMAND
UNITED STATES AIR FORCE

NOTICE AND SIGNATURE PAGE

Using Government drawings, specifications, or other data included in this document for any purpose other than Government procurement does not in any way obligate the U.S. Government. The fact that the Government formulated or supplied the drawings, specifications, or other data does not license the holder or any other person or corporation; or convey any rights or permission to manufacture, use, or sell any patented invention that may relate to them.

Qualified requestors may obtain copies of this report from the Defense Technical Information Center (DTIC) (http://www.dtic.mil).

AFRL-RX-WP-JA-2015-0104 HAS BEEN REVIEWED AND IS APPROVED FOR PUBLICATION IN ACCORDANCE WITH ASSIGNED DISTRIBUTION STATEMENT.

//Signature//

MICHEAL E. BURBA, Project Engineer
Metals Branch
Structural Materials Division

//Signature//

DANIEL J. EVANS, Chief
Metals Branch
Structural Materials Division

//Signature//

ROBERT T. MARSHALL, Deputy Chief
Structural Materials Division
Materials And Manufacturing Directorate

This report is published in the interest of scientific and technical information exchange and its publication does not constitute the Government's approval or disapproval of its ideas or findings.

REPORT DOCUMENTATION PAGE

Form Approved
OMB No. 0704-0188

1. REPORT DATE *(DD-MM-YY)*	2. REPORT TYPE	3. DATES COVERED *(From - To)*
April 2014	Interim	19 March 2014 – 31 March 2014

4. TITLE AND SUBTITLE

A CRYSTAL-PLASTICITY FEM STUDY ON EFFECTS OF SIMPLIFIED GRAIN REPRESENTATION AND MESH TYPES ON MESOSCOPIC PLASTICITY HETEROGENEITIES (POSTPRINT)

5a. CONTRACT NUMBER
In-house

5b. GRANT NUMBER

5c. PROGRAM ELEMENT NUMBER
62102F

6. AUTHOR(S)

M.A. Groeber, T.J. Turner, D.M. Dimiduk, C.F. Woodward, and M.D. Uchic - AFRL/RXCM
Y.S. Choi and T.A. Parthasarathy - UES, Inc.

5d. PROJECT NUMBER
4349

5e. TASK NUMBER

5f. WORK UNIT NUMBER
X0W6

7. PERFORMING ORGANIZATION NAME(S) AND ADDRESS(ES)

AFRL/RXCM
2941 Hobson Way
Bldg 654, Rm 136
Wright-Patterson AFB, OH 45433

UES Inc.
4401 Dayton-Xenia Rd.
Dayton, OH 45432-1894

8. PERFORMING ORGANIZATION REPORT NUMBER

9. SPONSORING/MONITORING AGENCY NAME(S) AND ADDRESS(ES)

Air Force Research Laboratory
Materials and Manufacturing Directorate
Wright-Patterson Air Force Base, OH 45433-7750
Air Force Materiel Command
United States Air Force

10. SPONSORING/MONITORING AGENCY ACRONYM(S)
AFRL/RXCM

11. SPONSORING/MONITORING AGENCY REPORT NUMBER(S)
AFRL-RX-WP-JA-2015-0104

12. DISTRIBUTION/AVAILABILITY STATEMENT

Distribution Statement A. Approved for public release; distribution unlimited.

13. SUPPLEMENTARY NOTES

Journal article published in *Materials Science and Engineering A*, 553 (2012), pp 37-44. This report contains color. The final publication is available at http://dx.doi.org/10.1016/j.msea.2012.05.089.

14. ABSTRACT

A numerical study using crystal plasticity finite element method was performed in order to investigate the influence of the grain boundary morphology (stair-case or smooth/flat) and the selection of different mesh types (hexahedral and tetrahedral meshes) on the distribution of simulated plasticity heterogeneities. A bicrystal (a hard grain and a soft grain) sphere embedded in a cubic grain was utilized to perform the current numerical study. The volume averaged responses for the simulated plasticity values (von Mises stress, total accumulated slip system shear and maximum accumulated slip system shear) showed no significant dependence on the grain boundary representation and mesh type. However, the bicrystal represented by uniform hexahedral meshes with stair-case grain boundaries tends to show more extreme local plasticity values (in the head and tail of the distribution), particularly populated in the grain boundary region. Differences in local plasticity values between the stair-case and the smooth (or flat) grain boundary cases and between the hexahedral and the tetrahedral mesh cases were largest in the grain boundary region, and the degree of the differences depended upon the plasticity susceptibility of the grain. The simulation results suggest that the grain boundary represented by the stair-case morphology can be a source and/or a sink for local extreme plasticity, compared to the grain boundary represented by the smooth (or flat) morphology.

15. SUBJECT TERMS

crystal plasticity, finite element method, mesoscopic plasticity, grain representation, mesh type

16. SECURITY CLASSIFICATION OF:			17. LIMITATION OF ABSTRACT:	18. NUMBER OF PAGES	19a. NAME OF RESPONSIBLE PERSON (Monitor)
a. REPORT	b. ABSTRACT	c. THIS PAGE			Micheal E. Burba
Unclassified	Unclassified	Unclassified	SAR	11	19b. TELEPHONE NUMBER *(Include Area Code)* (937) 255-9795

Materials Science and Engineering A 553 (2012) 37–44

Contents lists available at SciVerse ScienceDirect

Materials Science and Engineering A

journal homepage: www.elsevier.com/locate/msea

A crystal-plasticity FEM study on effects of simplified grain representation and mesh types on mesoscopic plasticity heterogeneities

Y.S. Choi[b,*], M.A. Groeber[a], T.J. Turner[a], D.M. Dimiduk[a], C. Woodward[a], M.D. Uchic[a], T.A. Parthasarathy[b]

[a] Air Force Research Laboratory, AFRL/RXLM, 2230 Tenth Street, Wright-Patterson AFB, OH 45433-7817, USA
[b] UES, Inc., 4401 Dayton-Xenia Rd., Dayton, OH 45432-1894, USA

ARTICLE INFO

Article history:
Received 2 April 2012
Received in revised form 25 May 2012
Accepted 28 May 2012
Available online 9 June 2012

Keywords:
Crystal plasticity
Finite element method
Mesoscopic plasticity
Grain representation
Mesh type

ABSTRACT

A numerical study using crystal plasticity finite element method was performed in order to investigate the influence of the grain boundary morphology (stair-case or smooth/flat) and the selection of different mesh types (hexahedral and tetrahedral meshes) on the distribution of simulated plasticity heterogeneities. A bicrystal (a hard grain and a soft grain) sphere embedded in a cubic grain was utilized to perform the current numerical study. The volume averaged responses for the simulated plasticity values (von Mises stress, total accumulated slip system shear and maximum accumulated slip system shear) showed no significant dependence on the grain boundary representation and mesh type. However, the bicrystal represented by uniform hexahedral meshes with stair-case grain boundaries tends to show more extreme local plasticity values (in the head and tail of the distribution), particularly populated in the grain boundary region. Differences in local plasticity values between the stair-case and the smooth (or flat) grain boundary cases and between the hexahedral and the tetrahedral mesh cases were largest in the grain boundary region, and the degree of the differences depended upon the plasticity susceptibility of the grain. The simulation results suggest that the grain boundary represented by the stair-case morphology can be a source and/or a sink for local extreme plasticity, compared to the grain boundary represented by the smooth (or flat) morphology.

1. Introduction

Crystal plasticity finite element method (CP-FEM) approaches have been widely used to model elasto-viscoplastic or plastic responses of polycrystalline metals at the mesoscopic scale, wherein deformation heterogeneities due to anisotropic responses of differently oriented grains are of main interest. In general, such mesoscopic CP-FEM approaches utilize 3D polycrystalline microstructures, which are synthetically generated using numerical tools [1–6], experimentally obtained using destructive or non-destructive techniques [7,8], or semi-empirically reconstructed from experimental 2D images [9–14]. Simulation results are usually analyzed in order to clarify the spatial distribution of stress (or strain) heterogeneities (or hot spots) [9,14,15], the statistics of extreme values of simulated plasticity [16] and its relation to microstructural features such as grain boundaries and precipitates (if present). Here, the heterogeneity of plasticity near grain boundaries draws particular attention since such regions can be susceptible to plasticity, depending upon the level of the deformation compatibility between the grains neighboring each other [14,17].

In reality, grain boundaries in polycrystalline metals are smooth with curvatures, based upon the energy balance from crystallography and chemistry between neighboring grains. 3D microstructures used for CP-FEM simulations, however, are mostly represented in uniform cubic meshes (or "voxels"), which causes grain morphologies inherently represented by "stair-case" boundaries. It is generally expected that simulated local plasticity responses can be different between 3D microstructures having stair-case grain boundaries and smooth (or flat) grain boundaries, particularly in the vicinity of grain boundaries. Furthermore, even for a 3D microstructure properly meshed to have smooth (or flat) grain boundaries, the choice of a mesh type, such as hexahedral and tetrahedral meshes, may also influence the distribution of simulated local plasticity responses. It is surprising to know that only a few numerical studies have been actually conducted to compare crystal plasticity responses between different grain boundary representations [4,5,18] and mesh types [19,20]. Even for those numerical studies, the comparison was limited to the global average response [5,18] and just qualitative local responses [4].

Increasing the mesh density can visually minimize stair-case boundaries of grains and improve the discrepancy in local plasticity

* Corresponding author. Tel.: +1 937 255 1995; fax: +1 937 656 7292.
E-mail address: ychoi@ues.com (Y.S. Choi).

0921-5093/$ – see front matter © 2012 Elsevier B.V. All rights reserved.
http://dx.doi.org/10.1016/j.msea.2012.05.089

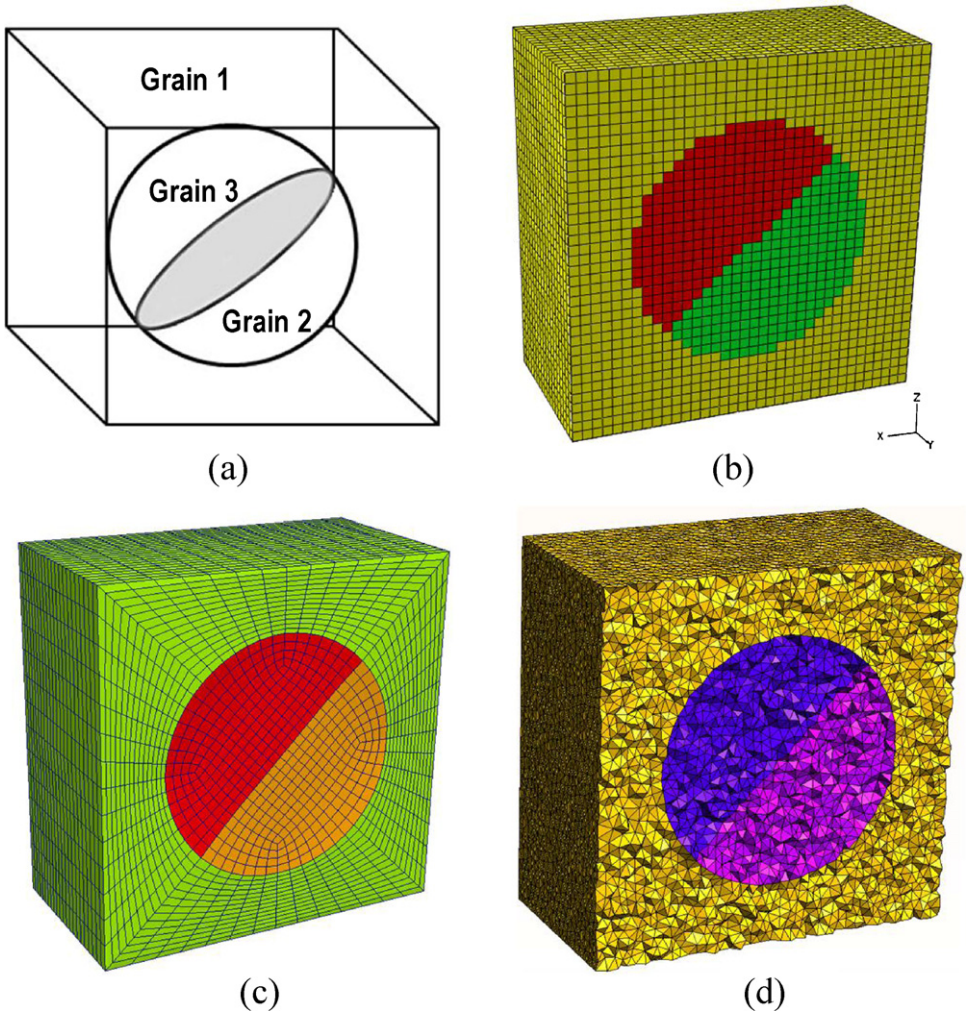

Fig. 1. (a) Schematic illustration of the tricrystal geometry used in the present study, and 3D cross-sectional views of the tricrystal differently represented by (b) hex-meshed stepped, (c) hex-meshed smooth and (d) tet-meshed smooth geometries, respectively.

responses between the smooth and the stepped cases [21] at a certain resolution window. However, this approach can have a prohibitive computational expense (in computation time and resources), and still does not address the fundamental issue associated with the difference in deformation compatibility and resulting heterogeneity between the smooth (or flat) and the stair-case boundaries. This issue and associated risks need to be clearly assessed and understood when the CP-FEM simulation is intended to study the statistics of hot spots and extreme values of plasticity. In the present study, preliminary CP-FEM simulations were performed using a simple tricrystal geometry (a bicrystal sphere embedded in a cubic grain) in order to gain basic understanding about differences in simulated mesoscopic plasticity responses and heterogeneities between 3D microstructures having differently represented grain boundary morphologies and mesh types.

2. Simulation details

A tricrystal geometry, which is a bicystal sphere embedded in a cubic grain, was generated for the current parametric CP-FEM study. Fig. 1(a) schematically illustrates the tricrystal geometry. A diagonally flat grain boundary was introduced to the bicrystal inside the cubic grain. The ratio between the diameter of the bicrystal sphere and the edge length of the cubic grain was maintained to be 2:3. The spherical bicrystal separated by the flat diagonal boundary is intended to investigate the difference in local plasticity responses when both curved and flat grain boundaries are represented by different topologies (smooth and stair-case topologies) and mesh types (hexahedral and tetrahedral elements). Fig. 1(b)–(d) shows 3D cross-sectional views of the tricrystal differently represented by (b) hex-meshed stepped, (d) hex-meshed smooth and (d) tet-meshed smooth geometries, respectively. For the generation of the stair-case geometry of the tricrystal shown in Fig. 1(b), the original geometry of Fig. 1(a) was superimposed on a $36 \times 36 \times 36$ hexahedral (uniform cubic) grid, and each hex-element was assigned to a corresponding grain, based upon its proximity to the grain. For the generation of smooth geometries of the tricrystal shown in Fig. 1(c) and (d), all three grains were meshed independently (with hexahedral and tetrahedral elements, respectively) while maintaining the smooth and diagonally flat boundaries, and the continuity of meshes across the boundary.

Fig. 2 shows the distribution of minimum dihedral angles ($\theta_{\min}$) for 3D mesh elements that constitute the bicrystal sphere represented by hex-meshed smooth (Fig. 1(c)) and tet-meshed smooth (Fig. 1(d)) geometries, respectively. Note that the dihedral angle for the perfect equilateral tetrahedron is 70.5°. In Fig. 2, the average $\theta_{\min}$ for tet- and hex-mesh elements is about 50° and 80°, respectively, and the smallest $\theta_{\min}$ are about 20° for tet-mesh elements and about 58° for hex-mesh elements. It indicates that quality hex- and tet-meshes were generated for smooth bicrystal geometries such that one can expect minimized numerical errors associated

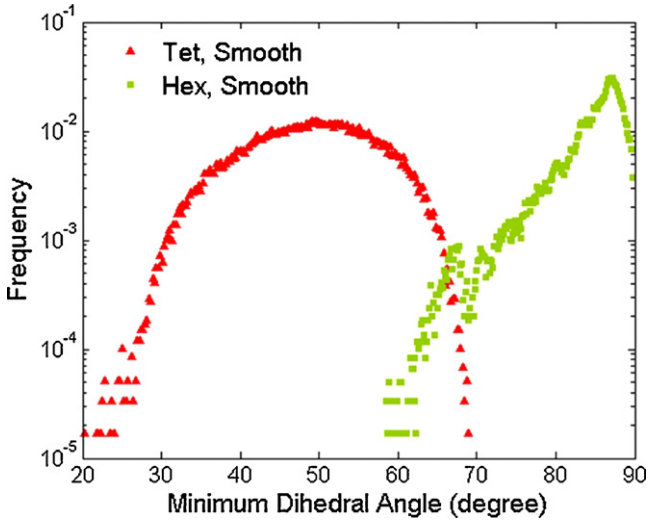

Fig. 2. Distribution of minimum dihedral angles for the bicrystal sphere represented by hex-meshed smooth (Fig. 1(c)) and tet-meshed smooth (Fig. 1(d)) geometries, respectively.

with poor quality mesh elements [22]. Also, an extra effort was made to mesh all cases in Fig. 1(b)–(d) to have a computationally comparable number of mesh elements such that the computational cost is of the same order for all cases. Total numbers of elements and corresponding integration points for each case are summarized in Table 1 for each grain. Here, linear elements (C3D8 for hexahedral and C3D4 for tetrahedral elements [22]) were used for CP-FEM simulations for all cases.

The elasto-viscoplastic constitutive model for FCC crystals was used in the present CP-FEM simulations. In particular, anisotropic elasto-viscoplasticity was applied to the bicrystal sphere (grains 2 and 3 in Fig. 1(a)), while isotropic elasto-viscoplasticity was used for the surrounding cubic grain (grain 1) in Fig. 1(a). For the anisotropic elasto-viscoplasticity constitutive model for grains 2 and 3 in Fig. 1(a), the power law and Voce-type parabolic hardening formulations were used to describe the slip system shear rate ($\dot{\gamma}^\alpha$) and the evolution of slip resistance ($\hat{g}$):

$$\dot{\gamma}^\alpha = \dot{\gamma}_o \left| \frac{\tau^\alpha}{\hat{g}} \right|^{1/m} sign(\tau^\alpha) \tag{1}$$

and

$$\dot{\hat{g}} = \theta_o \frac{\hat{g}_s - \hat{g}}{\hat{g}_s - \hat{g}_o} \sum_\alpha \left| \dot{\gamma}^\alpha \right| \tag{2}$$

where, $\dot{\gamma}_o$, τ^α and m are the reference shear rate, the resolved shear stress on the slip system α and the strain rate sensitivity parameter, respectively. In Eq. (2), θ_o, $\hat{g}_o$ and $\hat{g}_s$ are the initial hardening rate, initial and final values of the slip resistance, respectively. Values of these parameters used in the present simulations are listed in Table 2. Here, C_{11}, C_{12} and C_{44} are elastic constants. Elastic constants in Table 2 were taken from those for pure nickel. However, all other input parameter values in Table 2 was arbitrarily chosen

Table 1
Total numbers of elements and integration points (in brackets) for the tricrystal.

	Hex-meshed stepped	Hex-meshed smooth	Tet-meshed smooth
Grain 2	3.6 (28.8)	3.7 (29.8)	29.5 (29.5)
Grain 3	3.6 (28.8)	3.7 (29.8)	29.4 (29.4)
Grain 1	39.4 (315.6)	38.4 (307.3)	321.1 (321.1)

In thousands.

Table 2
Values of input parameters used for anisotropic elasto-viscoplasticity (grains 2 and 3).

$\dot{\gamma}_o$	0.001 s^{-1}
m	0.03
$\hat{g}_o$	200 MPa
$\hat{g}_s$	400 MPa
θ_o	500 MPa
C_{11}	247 GPa
C_{12}	147 GPa
C_{44}	125 GPa

to represent a FCC crystal. For isotropic elasto-viscoplasticity for grain 1 in Fig. 1(a), values for C_{11}, C_{12} and C_{44} were given as 344, 147 and 98 GPa, respectively, such that the elastic anisotropy factor ($A = C_{44}/0.5(C_{11} - C_{12})$) becomes 1 for isotropic elasticity. Upon plasticity, slip rate ($\dot{\gamma}^\alpha$) was set to be equal for all twelve slip systems in order to achieve isotropic plasticity – strictly speaking, isotropic plasticity used in the present model is limited to isotropic plastic flow for twelve slip systems of a FCC crystal.

Constitutive models described above were implemented in the commercial finite element package ABAQUS® through the User MATerial subroutine UMAT [22]. Simple tension (along the vertical direction in Fig. 1(a)) boundary conditions were applied to all simulation cases given in Fig. 1(b) and (c), with the strain rate, 0.0001 s^{-1}, up to the target axial strain, 0.6%. Here, grain 2 and grain 3 in Fig. 1(a) are oriented such that their [$\bar{1}$ 1 1] and [$\bar{1}$ 2 3] crystallographic directions are parallel to the tensile direction, respectively. This sets grains 2 and 3 as plastically hard and soft, respectively (when pulled along the tensile direction). Results from all simulation cases (Fig. 1(b)–(d)), particularly for grains 2 and 3, were quantitatively compared by their volume averaged global responses, the statistical distribution, and upper and lower plasticity values (*viz.*, hot and cold spots). Here, three selected parameters, the von Mises stress (σ_M), the total accumulated plastic shear strain ($\Sigma\gamma^\alpha$) from all slip systems, and the maximum slip shear strain accumulated in a slip system (γ^α_{max}) were chosen to compare local plasticity values between the cases. For the calculation of $\Sigma\gamma^\alpha$ the increment of slip system shear ($\Delta\gamma^\alpha$) was summed over all twelve slip systems at each simulation time step ($|\Sigma\Delta\gamma^\alpha|_{\Delta t}$), and $\Sigma\gamma^\alpha$ was determined by the summation of all $|\Sigma\Delta\gamma^\alpha|_{\Delta t}$'s.

3. Simulation results and discussion

Fig. 3(a)–(c) shows responses of σ_M, $\Sigma\gamma^\alpha$ and γ^α_{max} values averaged over grains 2 and 3, respectively, as a function of the global axial strain for hex-meshed stepped, smooth and tet-meshed smooth cases. In Fig. 3(a) σ_M values averaged over all three grains were also plotted as a function of the global axial strain for comparison. The simulation result shows no significant differences in grain-averaged σ_M, $\Sigma\gamma^\alpha$ and γ^α_{max} responses as a function of the global axial strain for all simulation cases. In Fig. 3(a), the σ_M response averaged over all three grains shows no sensitivity to the choice of stair-case or smooth grain boundaries and hexahedral or tetrahedral meshes. The maximum percentage difference in grain-averaged σ_M, $\Sigma\gamma^\alpha$ and γ^α_{max} values at 0.6% axial strain was 0.4%, 3% and 3.3% for grain 2 and 1%, 0.7% and 1% for grain 3, respectively. The results clearly show that the average responses of simulated σ_M, $\Sigma\gamma^\alpha$ and γ^α_{max} values are not significantly influenced by the selection of the grain boundary representation (stair-case or smooth boundaries) or the mesh type (hexahedral or tetrahedral meshes). The statistical distribution of all simulated σ_M, $\Sigma\gamma^\alpha$ and γ^α_{max} values (taken from all integration points) at 0.6% strain for grains 2 and 3 is plotted in a semi-log scale in Fig. 4 for hex-meshed stepped, hex-meshed smooth and tet-meshed smooth cases. In Fig. 4, the statistical distribution of σ_M, $\Sigma\gamma^\alpha$, γ^α_{max} values is

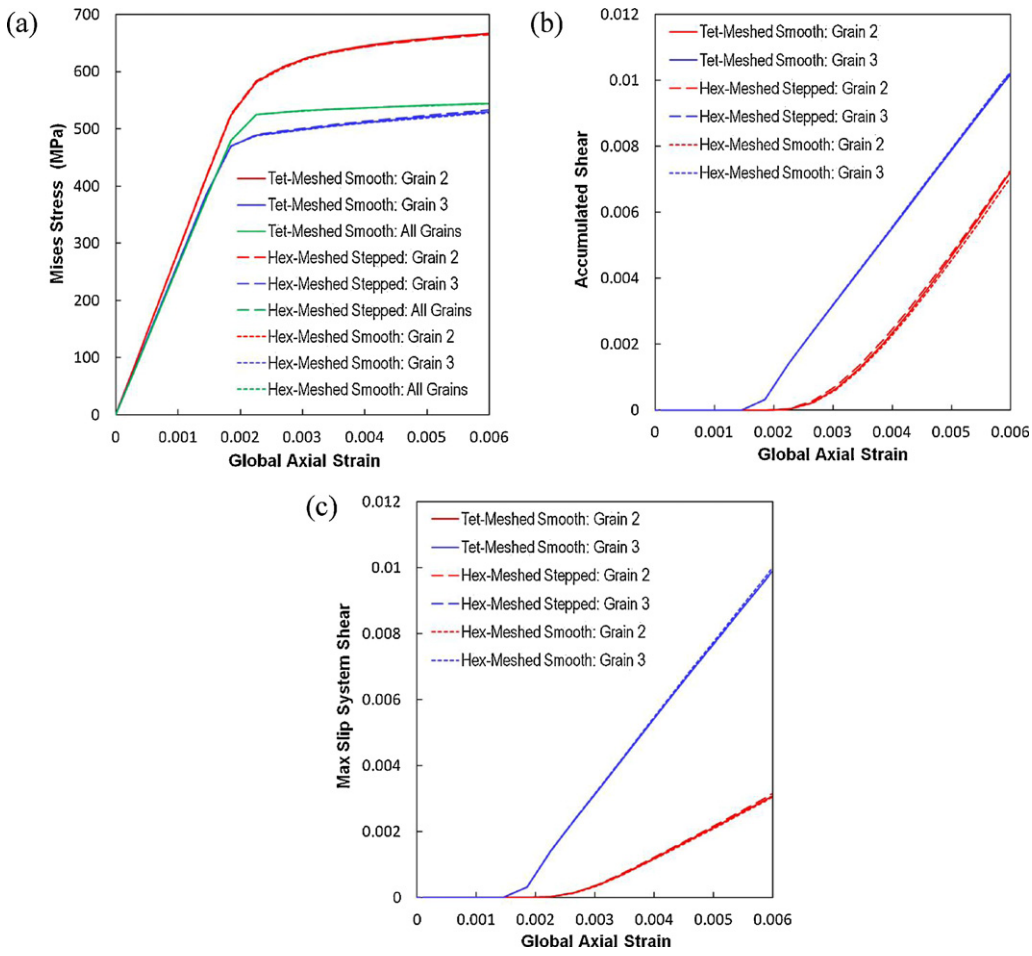

Fig. 3. Simulated volume averaged responses of (a) von Mises stress, (b) total accumulated shear strain, and (c) maximum slip system shear strain as a function of global axial strain.

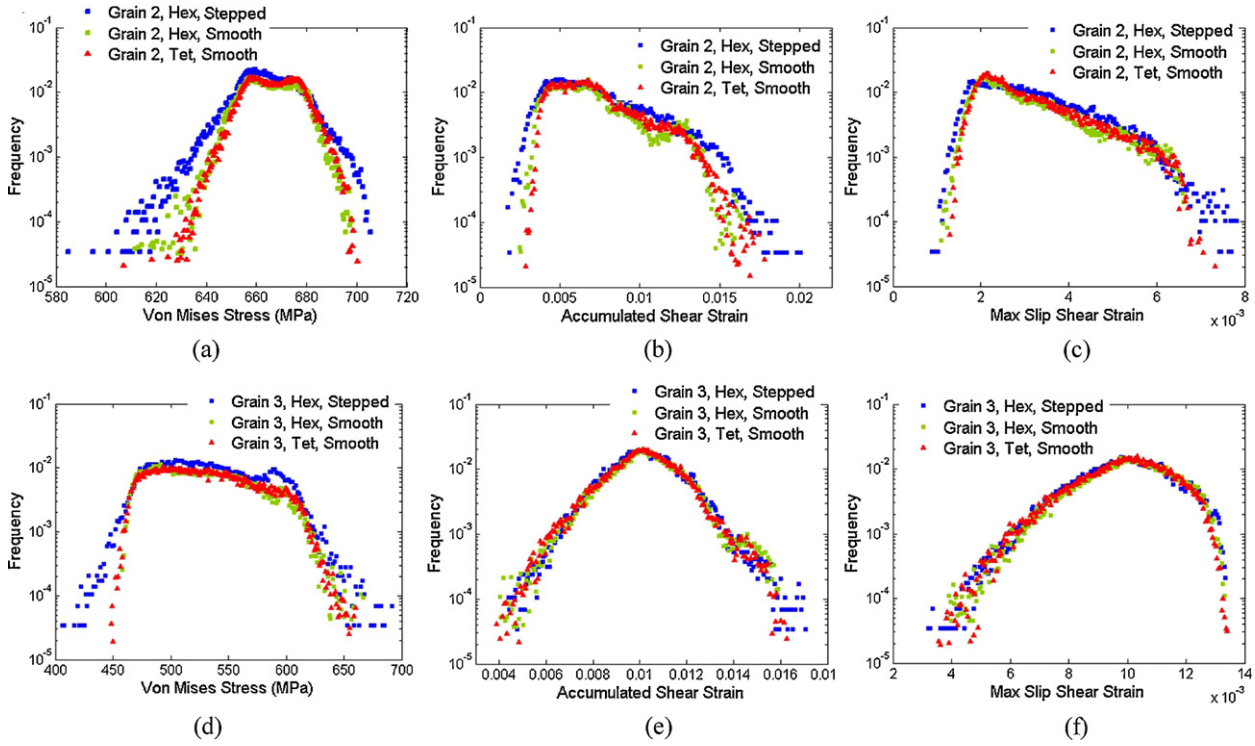

Fig. 4. Statistical distribution of all simulated σ_M, $\Sigma\gamma^\alpha$, γ^α_{max} values (taken from all integration points), as semi-log plots, for grain 2 ((a)–(c)) and for grain 3 ((d)–(f)) for hex-meshed stepped, hex-meshed smooth and tet-meshed smooth cases at 0.6% strain.

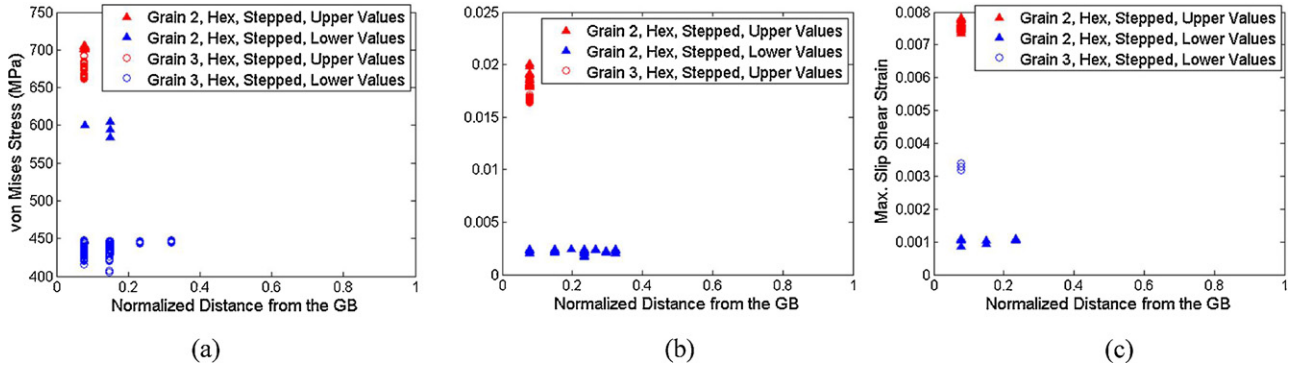

Fig. 5. All extreme values of (a) σ_M, (b) $\Sigma\gamma^\alpha$ and (c) γ^α_{max} (from Fig. 4) plotted as a function of the normalized distance from the grain boundary for the hex-meshed stepped grains 2 and 3. The normalized distance from the grain boundary was determined by normalizing the calculated grain boundary distances with the maximum grain boundary distance.

very similar between the hex-meshed smooth (green squares) and the tet-meshed smooth (red triangles) cases. However, the hex-meshed stepped case (blue squares) tends to show more excessive σ_M, $\Sigma\gamma^\alpha$ and γ^α_{max} values, both in the tail and head of the distribution, compared to the hex-meshed and tet-meshed smooth cases. These excessive cold and hot (extreme) spots in the hex-meshed stepped case are particularly apparent for the σ_M, $\Sigma\gamma^\alpha$ and γ^α_{max} distribution in grain 2 (Fig. 4(a)–(c)), and the σ_M distribution in grain 3 (Fig. 4(d)). The $\Sigma\gamma^\alpha$ and γ^α_{max} distribution in grain 3 (Fig. 4(e)–(f)) is almost identical for the hex-meshed stepped, hex-meshed smooth and tet-meshed smooth cases.

The results from Fig. 4 indicate that a grain represented by stair-case grain boundaries can cause excessively low and/or high local plasticity values, compared to a grain represented by smooth (or flat) grain boundaries. The presence of these excessive extreme values depends upon the plastic susceptibility of the grain and the choice of a plasticity parameter. In order to clarify how these extreme plasticity values are spatially distributed in the hex-meshed stepped grains, all extreme σ_M, $\Sigma\gamma^\alpha$ and γ^α_{max} values, which are smaller (or larger) than the minimum (or maximum) values for the hex-meshed and tet-meshed smooth cases, were plotted as a function of the normalized distance from the grain boundary in Fig. 5. Here, volume fractions of these excessive upper and lower extreme values found in the hex-meshed stepped grains were less than 1%. It is clear in Fig. 5 that all upper extreme σ_M, $\Sigma\gamma^\alpha$ and γ^α_{max} values in the hex-meshed stepped grains are distributed very near to the grain boundary, as are most of the lower extreme values.

It seems to be apparent from Figs. 4 and 5 that the hex-meshed stepped grain geometry tends to have upper and lower extreme spots of selected parameters that exceed those from the hex-meshed and tet-meshed smooth grain geometries. Also, these extreme spots were mainly found near the grain boundaries. This implies that local plasticity values can be underestimated or overestimated in the grain boundary region when the grain is represented by stair-case boundaries, in comparison to the cases that the grain is represented by smooth (or flat) boundaries. The degree of the underestimation and overestimation seems to be dependent upon how the deformation compatibility interacts between neighboring grains in the stair-case boundary region. Here, a quantitative comparison of local plasticity values between the cases is expected to provide the useful information. However, the exact point-to-point quantitative comparison in plasticity parameter values between the stepped and the smooth grain geometries is not feasible because local grain boundary regions occupied by the stepped grain and the smooth grain are different. To roughly estimate the local plasticity parameter value differences between the cases, the nearest point-based selected-parameter value comparison was performed for the hex-meshed stepped and hex-meshed smooth grain geometries, and for the hex-meshed smooth and tet-meshed smooth grain geometries. In Fig. 6 the average percentage differences in local selected-parameter values between the hex-meshed stepped and hex-meshed smooth cases (Fig. 6(a)–(c)), and between the hex-meshed smooth and the tet-meshed smooth cases (Fig. 6d–f), are plotted as a function of normalized distance from the grain boundary for grain 2 (closed symbols) and grain 3 (open symbols) at 0.6% strain. In Fig. 6(a)–(c), the figure legend "Hex, Stepped > Hex, Smooth" (or "Hex, Stepped < Hex, Smooth") indicates the average percentage difference profiles (plotted as a function of normalized distance from the grain boundary) for all local σ_M, $\Sigma\gamma^\alpha$ and γ^α_{max} values whose magnitudes are larger (or smaller) in the hex-meshed stepped geometry than in the hex-meshed smooth geometry. The same notation applies to the figure legend "Hex, Smooth > Tet, Smooth" and "Hex, Smooth < Tet, Smooth" in Fig. 6(d)–(f). Here, several things need to be pointed out from Fig. 6.

First, the average percentage differences in local plasticity values (hereafter, for simplicity these will be referred to as $\Delta\sigma_M$, $\Delta\Sigma\gamma^\alpha$ and $\Delta\gamma^\alpha_{max}$ for average percentage differences in local σ_M, $\Sigma\gamma^\alpha$ and γ^α_{max} values between the cases, respectively) tend to be larger in the grain boundary region, compared to those in the grain interior region, for all comparison cases. This trend is understandable when comparing local plasticity differences between the hex-meshed stepped and the hex-meshed smooth cases, since the mesh morphological difference is greatest only along the grain boundary. Perhaps, the different deformation incompatibility associated with different grain boundary morphologies leads to different local plasticity responses between the two cases. $\Delta\Sigma\gamma^\alpha$ and $\Delta\gamma^\alpha_{max}$ values are as large as about 70% in the grain boundary region in Fig. 6(b) and (c). However, a similar trend was also shown for $\Delta\sigma_M$, $\Delta\Sigma\gamma^\alpha$ and $\Delta\gamma^\alpha_{max}$ between the hex-meshed smooth and the tet-meshed smooth cases (Fig. 6(d)–(f)), even though $\Delta\sigma_M$, $\Delta\Sigma\gamma^\alpha$ and $\Delta\gamma^\alpha_{max}$ values are much smaller for this comparison. This indicates that the deformation constraint and associated deformation incompatibility near the grain boundary lead to different local plasticity responses between the hex-meshed smooth and the tet-meshed smooth grains. Here, the $\Delta\Sigma\gamma^\alpha$ and $\Delta\gamma^\alpha_{max}$ values are as large as 10% in the grain boundary region (Fig. 6(e) and (f)).

Second, $\Delta\sigma_M$, $\Delta\Sigma\gamma^\alpha$ and $\Delta\gamma^\alpha_{max}$ values are sensitive to the plastic properties of the grain. For all comparison cases, $\Delta\Sigma\gamma^\alpha$ and $\Delta\gamma^\alpha_{max}$ values are larger in grain 2 (multi-slip oriented hard grain when pulled along the tensile direction) than those in grain 3 (single slip oriented soft grain when pulled along the tensile direction), while $\Delta\sigma_M$ values are larger in grain 3 than those in grain 2. When compared to the hard grain, the soft grain tends to accommodate local deformation gradients in an efficient fashion that minimizes $\Delta\Sigma\gamma^\alpha$ and $\Delta\gamma^\alpha_{max}$ between stepped and smooth

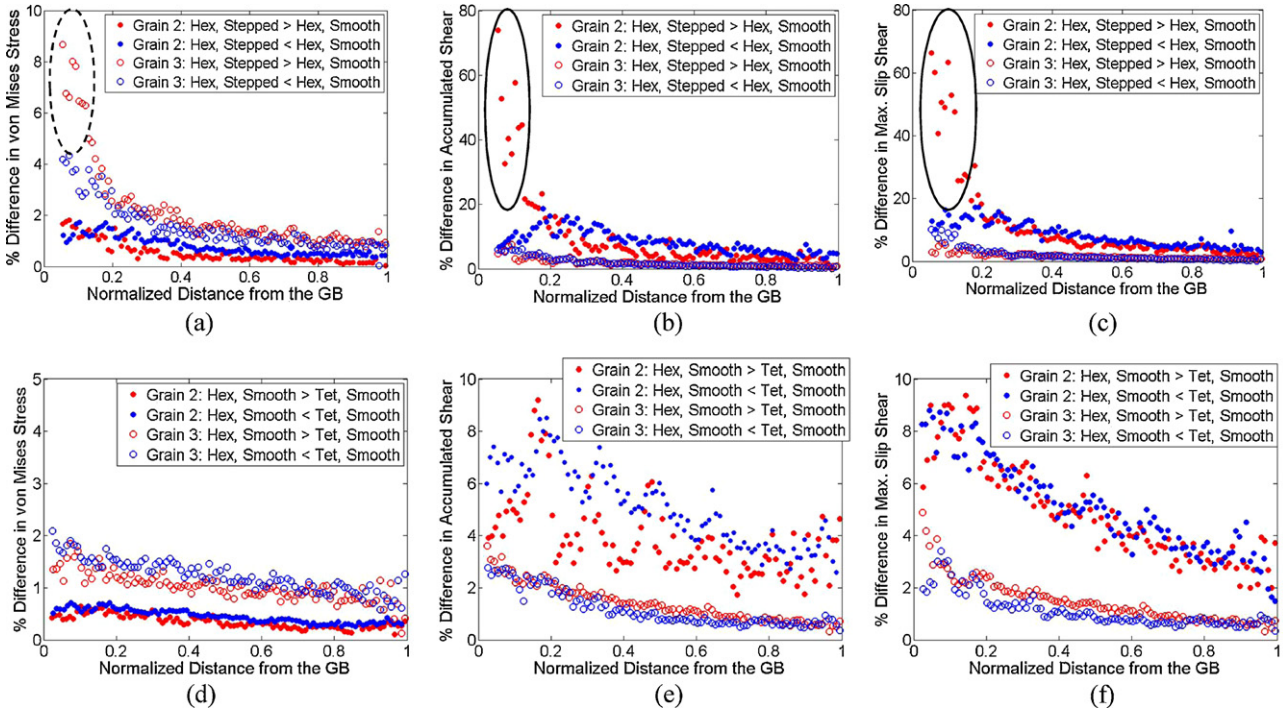

Fig. 6. Average percentage differences in local σ_M, $\Sigma\gamma^\alpha$, γ^α_{max} values between the hex-meshed stepped and hex-meshed smooth grains 2 and 3 ((a)–(c)) and between the hex-meshed smooth and tet-meshed smooth grains 2 and 3 (d–f) as a function of the normalized distance from the grain boundary at 0.6% strain.

grains and between hex-meshed and tet-meshed grains. In the hard grain, however, the local deformation incompatibility associated with stair-case boundaries seems to be accommodated by inducing intense plasticity activity in the local grain boundary region. This is probably why $\Delta\Sigma\gamma^\alpha$ and $\Delta\gamma^\alpha_{max}$ values are very large (particularly, larger $\Sigma\gamma^\alpha$ and γ^α_{max} values in the stepped grain boundary region, as indicated by solid circles in Fig. 6(b) and (c)) in grain 2. In Fig. 6, however, $\Delta\sigma_M$ values show the opposite trend – larger in the soft grain (grain 3) than in the hard grain (grain 2 in Fig. 6(a) and (d)). The elastic anisotropy (A = 2.5 for grains 2 and 3) and associated elastic interactions was initially suspected to play a role in determining $\Delta\sigma_M$ values for the soft and hard grains – for reference, the calculated elastic moduli for grains 2 and 3 are 305 and 234 GPa, respectively. However, in Fig. 7 $\Delta\sigma_M$ values are compared in the fully elastic regime (at 0.15% strain), and these show no significant difference between grains 2 and 3. This means that the $\Delta\sigma_M$ difference between hard and soft grains in Fig. 6(a) and (d) arises in the plastic regime. For the soft grain (grain 3) in Fig. 6, $\Delta\sigma_M$, $\Delta\Sigma\gamma^\alpha$ and $\Delta\gamma^\alpha_{max}$ values are in the same range (up to about 10% for the hex-meshed stepped and hex-meshed smooth grain comparison and up to about 5% for the hex-meshed and tet-meshed smooth grain comparison), implying that $\Delta\Sigma\gamma^\alpha$ and $\Delta\gamma^\alpha_{max}$ tie directly to $\Delta\sigma_M$. For the hard grain (grain 2), however, $\Delta\sigma_M$ values are far smaller than $\Delta\Sigma\gamma^\alpha$ and $\Delta\gamma^\alpha_{max}$ values (up to about 70% $\Delta\Sigma\gamma^\alpha$ and $\Delta\gamma^\alpha_{max}$ and about 2% $\Delta\sigma_M$ for the hex-meshed stepped and hex-meshed smooth grain comparison, and up to about 10% $\Delta\Sigma\gamma^\alpha$ and $\Delta\gamma^\alpha_{max}$ and about 1% $\Delta\sigma_M$ for the hex-meshed and tet-meshed smooth grain comparison). This means that local σ_M responses (perhaps, related local stress state responses) in the hard grain seem to be far less sensitive to the grain boundary morphology and mesh type, compared to the $\Sigma\gamma^\alpha$ and γ^α_{max} sensitivities to the grain boundary morphology and mesh type in the hard grain. This actually results in smaller $\Delta\sigma_M$ values in the hard grain than in the soft grain (Fig. 6(a) and (d)).

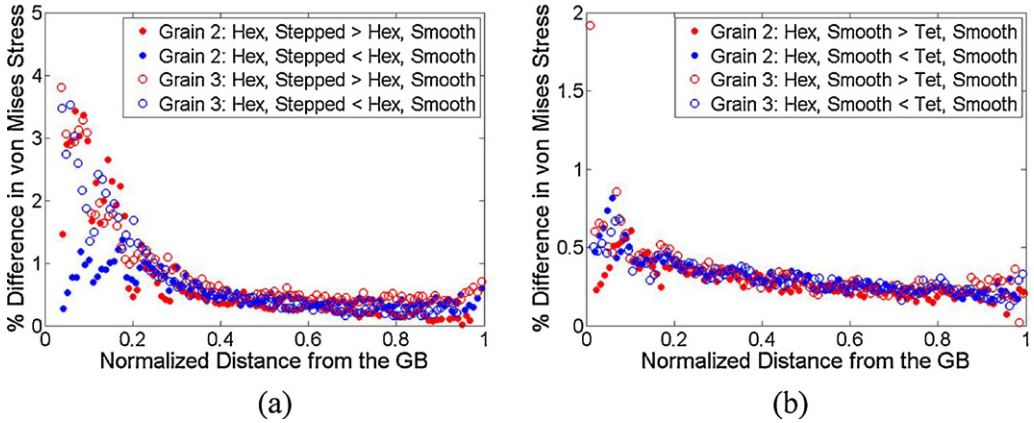

Fig. 7. Average percentage differences in local σ_M values (in the elastic regime) (a) between the hex-meshed stepped and hex-meshed smooth grains 2 and 3 and (b) between the hex-meshed smooth and tet-meshed smooth grains 2 and 3 as a function of the normalized distance from the grain boundary at 0.15% strain.

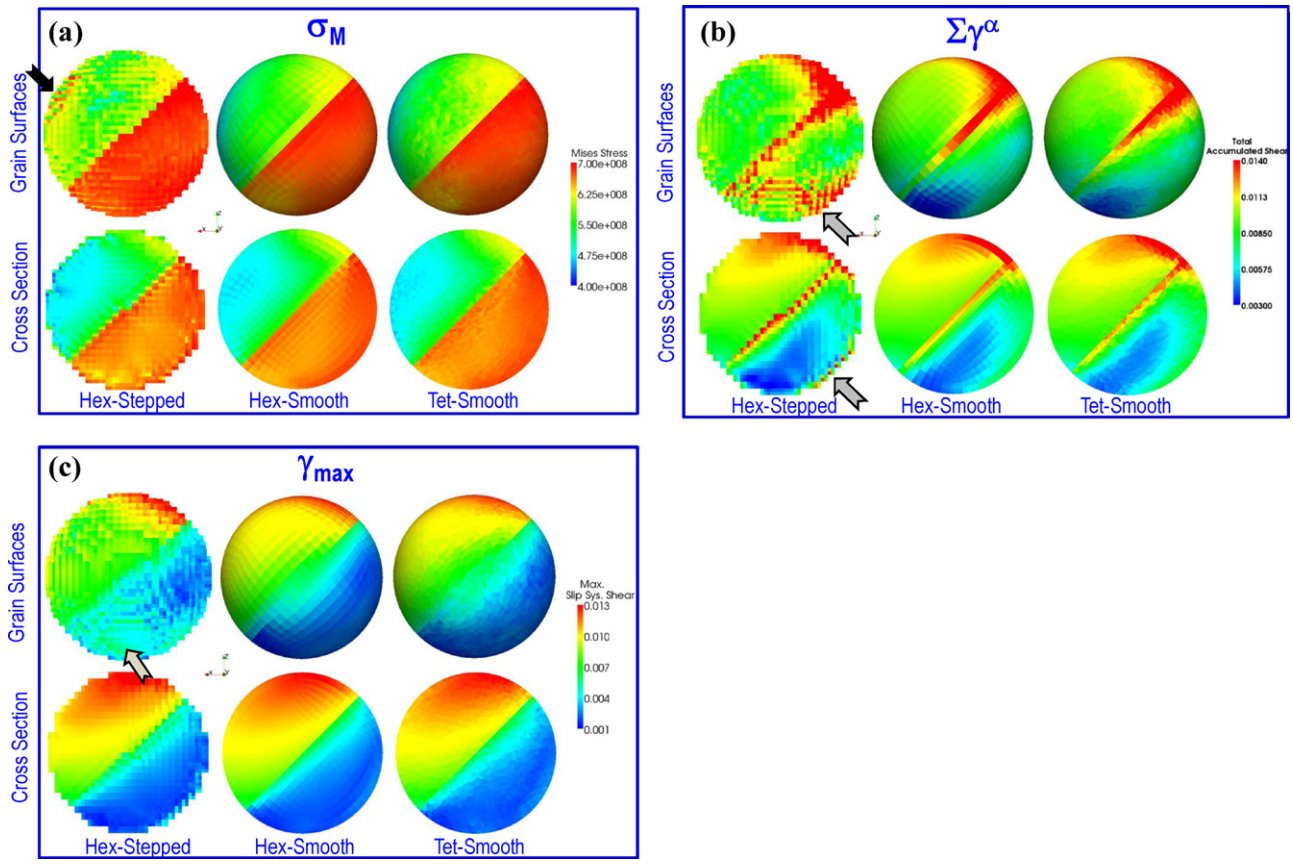

Fig. 8. Simulated bicrystal spheres visualized by (a) σ_M, (b) $\Sigma\gamma^\alpha$ and (c) γ^α_{max} for the hex-meshed stepped and hex-meshed smooth and tet-meshed smooth cases.

As previously mentioned, $\Delta\sigma_M$, $\Delta\Sigma\gamma^\alpha$ and $\Delta\gamma^\alpha_{max}$ values significantly increased in the grain boundary region (as indicated by broken and solid circles in Fig. 6), compared to the grain interior. All simulated bicrystal spheres were visualized by their plasticity parameter values in order to locate such spots with large $\Delta\sigma_M$, $\Delta\Sigma\gamma^\alpha$ and $\Delta\gamma^\alpha_{max}$ values. Fig. 8 shows the grain surface and cross-sectional views of σ_M, $\Sigma\gamma^\alpha$ and γ^α_{max} for all simulated bicrystal cases at 0.6% strain. Fig. 8 shows that very large $\Delta\Sigma\gamma^\alpha$ and $\Delta\gamma^\alpha_{max}$ values in grain 2 (indicated by solid circles in Fig. 6(b) and (c)) are mainly distributed near the grain boundary region between grain 2 and grain 1, as indicated by gray arrows in Fig. 8(b) and (c). Similarly, large $\Delta\sigma_M$ values in grain 3 (indicated by a broken circle in Fig. 6(a)) were found near the grain boundary region between grains 3 and 1, as indicated by a black arrow in Fig. 8(a). Also, note from Fig. 8 that the overall global contours of σ_M, $\Sigma\gamma^\alpha$ and γ^α_{max} appear to be similar between the simulation cases, even though local gradients of σ_M, $\Sigma\gamma^\alpha$ and γ^α_{max} are somewhat different location by location between the simulation cases.

4. Concluding remarks

In the present study, parametric CP-FEM simulations were performed using a bicrystal (a soft grain and a hard grain) sphere embedded in a cubic grain in order to investigate and compare global and local plasticity responses when the bicrystal sphere is represented by either uniform hexahedral (cubic) meshes with stair-case grain boundaries, non-uniform hexahedral meshes with smooth (or flat) grain boundaries or tetrahedral meshes with smooth (or flat) grain boundaries. Almost no differences are found in global averages of σ_M, $\Sigma\gamma^\alpha$ and γ^α_{max} responses for all simulation cases (Fig. 3), suggesting that the choice of the smooth or stair-case grain boundaries and the hexahedral or tetrahedral meshes has a minimal influence on global average responses at the selected strains. However, the statistical distribution of σ_M, $\Sigma\gamma^\alpha$ and γ^α_{max} values showed that the hex-meshed stepped case causes more extreme-value spots near tail and head of the distribution (Fig. 4). These extreme spots were heavily populated in the grain boundary region (Fig. 5), which is probably indicative of stair-case grain boundaries as a source and/or a sink for excessive local extreme plasticity. Also, note that the degree of the presence of those extreme spots in the hex-meshed stepped case depended upon the susceptibility of the grain to plasticity.

Larger $\Delta\Sigma\gamma^\alpha$ and $\Delta\gamma^\alpha_{max}$ values in the hard grain (grain 2 in Fig. 6(b), (c), (e) and (f)) indicates that the sensitivities of simulated local $\Sigma\gamma^\alpha$ and γ^α_{max} responses to the choice of smooth or stair-case boundaries and hexahedral or tetrahedral meshes are stronger in a hard grain than in a soft grain. However, the soft grain showed consistent $\Delta\sigma_M$, $\Delta\Sigma\gamma^\alpha$ and $\Delta\gamma^\alpha_{max}$ sensitivities to the choice of the smooth or stair-case grain boundaries and the hexahedral or tetrahedral meshes, while in the hard grain the $\Delta\sigma_M$ sensitivity is significantly smaller than $\Delta\Sigma\gamma^\alpha$ and $\Delta\gamma^\alpha_{max}$ sensitivities to the choice of the grain boundary representation and the mesh type. Perhaps, the further numerical study is needed to clarify the inconsistency between the $\Delta\sigma_M$ sensitivity and the $\Delta\Sigma\gamma^\alpha$ and $\Delta\gamma^\alpha_{max}$ sensitivities in the hard grain. As expected, the $\Delta\sigma_M$, $\Delta\Sigma\gamma^\alpha$ and $\Delta\gamma^\alpha_{max}$ values between the hex-meshed smooth and the tet-meshed smooth grains (Fig. 6(d)–(f)) were fairly small, when compared to those between the hex-meshed stepped and hex-meshed smooth grains (Fig. 6(a)–(c)). However, even for the former comparison, the simulated average local value difference was as large as 10% in $\Sigma\gamma^\alpha$ and γ^α_{max} and 2% in σ_M. Also, the largest local value difference was found in the grain boundary region for all comparisons.

Lastly, note that the current study is limited to comparing plasticity responses at the relatively early stage of plasticity (at 0.6% axial strain), *viz.* the viscoplastic regime. Comparing Fig. 7 with Fig. 6(a) and (d) indicates that the trend in $\Delta\sigma_M$ between different grain boundary representations and mesh types is different in the fully elastic regime and in the viscoplastic regime. It would be worthwhile to investigate how the trend in $\Delta\sigma_M$, $\Delta\Sigma\gamma^\alpha$ and $\Delta\gamma^\alpha_{max}$ between different grain boundary representations and the mesh types changes at a large plastic strain, which is the case for metal forming simulations. Such a numerical study would provide useful information for evaluating the sensitivity of local plasticity responses to different choices of the grain boundary representations and mesh types in metal forming simulations.

Acknowledgements

This work was supported by the contract research at the AFRL/RXLM under the U.S. Air force contract # FA8650-10-D-5226 (Y.S.C. and T.A.P.). The authors are grateful to Dr. R.A. Brockman of University of Dayton Research Institute for the fruitful discussion throughout the project. Computations were performed using computer resources at the Ohio Supercomputer Center (grant #'s PAS0647) and at the U.S. Air Force Research Laboratory DoD Supercomputing Resource Center (AFRL-DSRC).

References

[1] F. Barbe, L. Decker, D. Jeulin, G. Cailletaud, Int. J. Plasticity 17 (2001) 513–536.
[2] F. Barbe, S. Forest, G. Cailletaud, Int. J. Plasticity 17 (2001) 537–563.
[3] O. Diard, S. Leclercq, G. Rousselier, G. Cailletaud, Comput. Mater. Sci. 25 (2002) 73–84.
[4] T. Kanit, S. Forest, I. Galliet, V. Mounoury, D. Jeulin, Int. J. Solid Struct. 40 (2003) 3647–3679.
[5] O. Diard, S. Leclercq, G. Rousselier, G. Cailletaud, Int. J. Plasticity 21 (2005) 691–722.
[6] R. Loge, M. Bernacki, H. Resk, L. Delannay, H. Digonnet, Y. Chastel, T. Coupez, Philos. Mag. 88 (2008) 3691–3712.
[7] A.C. Lewis, M.A. Siddiq Qidwai, A.B. Geltmacher, Metall. Mater. Trans. A 41 (2010) 2522–2531.
[8] M.A. Siddiq Qidwai, A.C. Lewis, A.B. Geltmacher, Acta Mater. 57 (2009) 4233–4247.
[9] Z. Zhao, M. Ramesh, D. Raabe, A.M. Cuitino, R. Radovitzky, Int. J. Plasticity 24 (2008) 2278–2297.
[10] E. Heripre, M. Dexet, J. Crepin, L. Gelebart, A. Roos, M. Bornert, D. Caldemaison, Int. J. Plasticity 23 (2007) 1512–1539.
[11] A. Musienko, A. Tatschl, K. Schmidegg, O. Kolednik, R. Pippan, G. Cailetaud, Acta Mater. 55 (2007) 4121–4136.
[12] A. Zeghadi, F. N'Guyen, S. Forest, A.-F. Gourgues, O. Bouaziz, Philos. Mag. 87 (2007) 1401–1424.
[13] A. Zeghadi, S. Forest, A.-F. Gourgues, O. Bouaziz, Philos. Mag. 87 (2007) 1425–1446.
[14] T.R. Bieler, P. Eisenlohr, F. Roters, D. Kumar, D.E. Mason, M.A. Crimp, D. Raabe, Int. J. Plasticity 25 (2009) 1655–1683.
[15] A. Rollett, R. Lebensohn, M. Groeber, Y. Choi, J. Li, G. Rohrer, Modell. Simul. Mater. Sci. Eng. 18 (2010) 074005.
[16] C. Przybyla, D. McDowell, Int. J. Plasticity 27 (2011) 1871–1895.
[17] F. Roters, P. Eisenlohr, L. Hantcherli, D.D. Tjahjanto, T.R. Bieler, D. Raabe, Acta Mater. 58 (2010) 1152–1211.
[18] J. Qian, Y. Zhang, W. Wang, A. Lewis, S.M. Qidwai, A. Geltmacher, Int. J. Numer. Meth. Eng. 82 (2010) 1406–1423.
[19] M. Anahid, P. Chakraborty, S. Ghosh, The Ohio State University, Unpublished internal research, 2009.
[20] I. Simonovski, L. Cizelj, N. Jaksic, Nucl. Eng. Des. 241 (2011) 1184–1190.
[21] G. Cailletaud, S. Forest, D. Jeulin, F. Feyel, I. Galliet, V. Mounoury, S. Quilici, Comput. Mater. Sci. 27 (2003) 351–374.
[22] Dassult Systems Simulia Corp., ABAQUS/Standard 6.9-1, 2009.